

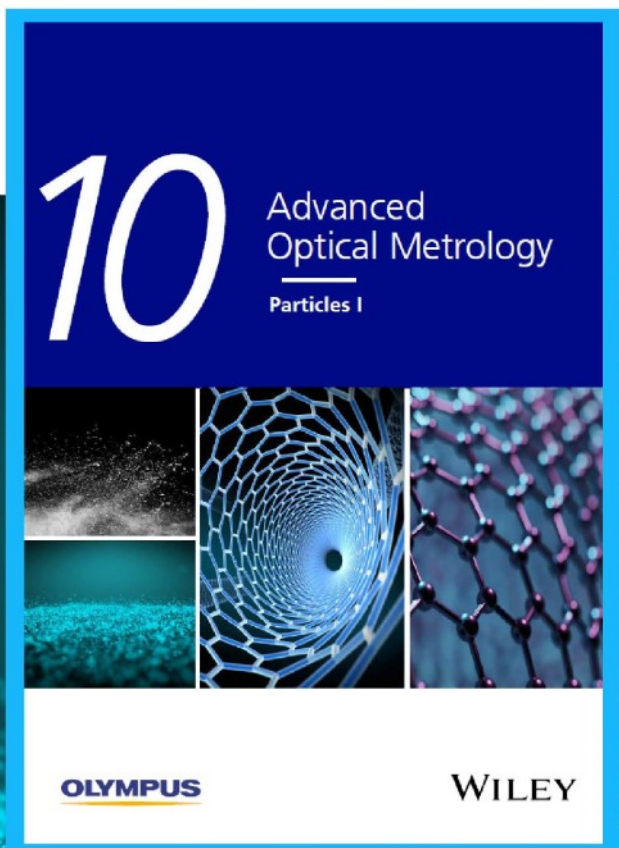


Particles I

Access the latest eBook →

Particles: Unique Properties,
Uncountable Applications

**Read the latest eBook and
better your knowledge with
highlights from the recent
studies on the design and
characterization of micro-
and nanoparticles for
different application areas.**



Access Now

This eBook is sponsored by

OLYMPUS

WILEY

A Functionally Stable RuMn Electrocatalyst for Oxygen Evolution Reaction in Acid

Lu An, Fan Yang, Cehuang Fu, Xiyang Cai, Shuiyun Shen, Guofeng Xia, Jing Li, Yunzhu Du, Liuxuan Luo, and Junliang Zhang*

Proton exchange membrane water electrolysis (PEMWE) is a key technology to solve the serious energy and environmental problems. However, the poor durability of electrocatalysts in acidic oxygen evolution reaction (OER) environment hinders the large-scale application of PEMWE. Herein, a robust RuMn electrochemical catalyst with a remarkable durability within 20 000 cyclic voltammetry cycles is reported. Furthermore, RuMn is stable for 720 h at 10 mA cm⁻² current density in 0.5 M H₂SO₄ solution with <100 mV overpotential increase, outperforming the most electrocatalysts reported to date, by far. An amorphous RuO_x shell is detected after the OER test, indicating a surface reconstruction process on the catalyst that inhibits steady-state dissolution. Further study demonstrates that the excellent durability of RuMn realized by protective RuO_x can be attributed to strong bond strength of Ru, which is supported by density functional theory calculations with high dissolution voltage. Thus, improving the bond strength of Ru extends the design strategy for the Ru-based alloy catalysts with considerable stability.

1. Introduction

Electrochemical water splitting is an effective energy storage technology of sustainable energies such as solar, wind, and tidal power by converting the intermittent energy into hydrogen.^[1] Proton exchange membrane water electrolysis (PEMWE) is a highly efficient energy conversion technology for high-purity hydrogen production. However, the key reaction for water electrolysis, oxygen evolution reaction (OER), requires high overpotential to overcome the sluggish kinetics of the 4-e⁻ transfer process.^[2] Due to the harsh acidic and anodic environment, only a few noble-metal-based OER electrocatalysts can remain stable under such circumstance, which hinders the

large-scale application of PEMWE. To date, Ir- and Ru-based catalysts are two benchmark materials for OER in acidic solutions,^[3] among which Ru-based materials have attracted increasing attention because of their higher electrochemical activity, less scarcity, and lower price compared with Ir. However, the stability of Ru-based catalysts remains a challenging issue because of their high steady-state dissolution rate during the OER process.^[1b]

Several possible mechanisms for the high dissolution rate of Ru-based catalysts were reported. A previous study by K Macounova declared that the steady-state dissolution is strongly correlated to the operation current, and therefore suggested the dissolution being related to the OER process.^[4] Further, studies revealed the reaction pathway of Ru preferring to lattice oxygen mechanism, indicating the

lattice oxygen in the RuO₂ takes part in OER to enhance activity but meanwhile, leads to oxidation of RuO₂ to soluble RuO₄.^[4-5] N Hodnik et al. observed transient dissolution of Ru at potentials lower than the OER potential (1.23 V vs RHE) and they deduced the catalytic instability of Ru, which can be induced by surface oxidation and reduction processes.^[6] All of the above studies indicate the significance of surface alteration on the dissolution. In this vein, the electrocatalytic stability of Ru-based materials could be enhanced by controlling the surface reconstruction.

Recently, surface engineering of noble-metal-based nanomaterials by doping alien atoms with dealloying treatment has received significant attention, which effectively boosts the durability and activity. Rather than directly catalyzing OER on their surface, pristine catalysts undergo surface transformation under OER electrocatalysis. Such controllable surface reconstruction represents a transition of pristine materials to accommodate the electrochemical environment through spontaneous alterations of atomic structure and electronic structure.^[7] A dynamically stable OER status would be achieved with the reconstructed surface as the real active sites during OER electrocatalysis. The surface structural transformation has been widely emphasized on OER materials in alkaline media, but less phenomenon have been detected in acidic OER catalysis.^[8] Single-atom such as Ir catalysts has been turned into a stable state and fixed by the formed shrinkage structure during the OER process with surface reconstruction.^[9] The state-of-the-art

L. An, F. Yang, C. Fu, X. Cai, S. Shen, G. Xia, J. Li, Y. Du, L. Luo, J. Zhang
Institute of Fuel Cells
School of Mechanical Engineering
Shanghai Jiao Tong University
Shanghai 200240, China
E-mail: junliang.zhang@sjtu.edu.cn

J. Zhang
MOE Key Laboratory of Power & Machinery Engineering
Shanghai Jiao Tong University
Shanghai 200240, China

 The ORCID identification number(s) for the author(s) of this article can be found under <https://doi.org/10.1002/adfm.202200131>.

DOI: 10.1002/adfm.202200131

OER catalyst $\text{IrO}_x/\text{SrIrO}_3$ was formed during electrochemical testing by Sr leaching from SrIrO_3 surface, which is the most stable Ir-based catalyst in acidic electrolyte for 30 h.^[8a] Mn shows advantages for both activity and stability for acidic OER. Mn has good stability as MnO_x itself, and also exhibits excellent stabilization effect when doped with IrRu or Ru.^[10] Even though the durability of OER catalysis for acidic media has substantially improved in these years, there is still a huge gap between existing performance and practical requirements.

Inspired by the surface reconstruction strategy, we synthesized Ru-based alloys by doping with Co, Cr, Zn, and Mn on carbon fiber papers (CFPs) with dealloying treatment. CV cycle test was applied as a surface transformation strategy that is also a preliminary screening for qualified OER catalysts. Among these Ru-based catalysts, RuMn alloy showed remarkable resistance to acid corrosion and overoxidation while other Ru-based samples (Ru, RuCo, RuCr, RuZn) deteriorated quickly in consecutive CV cycles. A surface reconstruction process was proved during the electrolysis along with Mn leaching, and an amorphous RuO_x surface was detected. In addition, RuMn catalyst was kept stable for 720 h in chronopotentiometry test at 10 mA cm^{-2} , substantially outperforming known catalysts in acidic environment. The formation of a robust amorphous surface may be attributed to the high bond strength of Ru in RuMn alloy, which is beneficial for the controllable reconstruction of Ru.

2. Results and Discussion

To determine the structure of samples, X-ray diffraction (XRD) patterns were detected. The diffractograms for Ru and Ru-M alloys (Figure 1) show that Ru-M alloys have the dominant peaks identical to those of Ru metal without characteristic peaks of doping metals, which confirms that no impure phases are formed. The diffraction peaks at 38.38° , 42.18° , 44.01° , 58.33° , 69.40° , and 78.39° can be indexed to (100), (002), (101), (102), (110), and (103) of Ru metal (PDF#65-7646), respectively. The peak at 54.2° referred to CFPs (Figure S1, Supporting Information). Upon addition of M (M = Cr, Zn, Mn, Co),

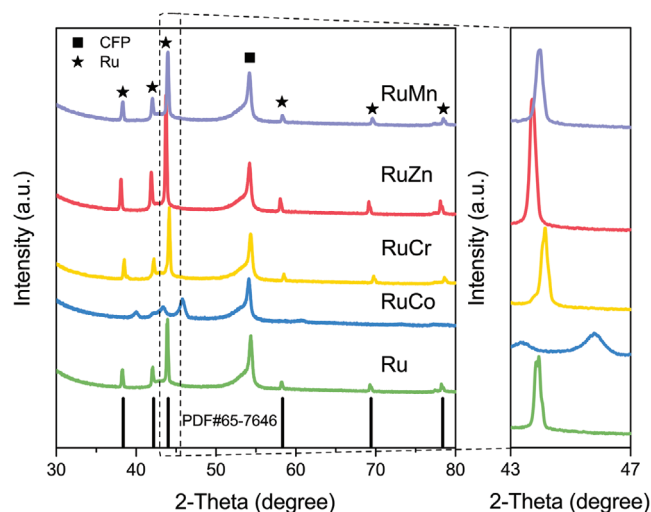


Figure 1. XRD patterns for Ru, RuCo, RuCr, RuZn, and RuMn.

gradual shifts of the Ru peaks toward higher diffraction angles are seen, which can be explained by contraction of the unit cell. It is worth noting that the broadened peaks of RuCo indicate the smaller size of the bimetallic alloys.

Morphologies of Ru-M alloys were investigated by scanning electron microscopy (SEM). Images of Ru-M alloy on CFPs were presented in Figure S2 (Supporting Information). Ru-M alloys particles were randomly distributed on carbon fibers. RuCo, RuCr, and RuZn nanoparticles were connected with larger particle bulks while Ru and RuMn alloys were shown as smaller bulk on carbon fibers. Most samples were connected tightly without obvious cracks, but RuMn alloy was shown as a porous structure. Energy-dispersive X-ray spectroscopy (EDS) analysis in Figure S3 (Supporting Information) had illustrated that Ruthenium atoms and doping atoms were evenly dispersed.

Before applying linear sweep voltammetry (LSV) evaluation of catalysts, electrochemistry should be stable after several cycles of CV measurement, which is also adopted as a dealloying process. All of the electrochemical tests were carried out in the O_2 -saturated $0.5 \text{ M H}_2\text{SO}_4$ electrolyte. CV cycles of Ru and Ru-M alloys between 1.25 and 1.75 V (vs reversible hydrogen electrode, RHE) are summarized in Figure 2. CV curves recorded on Ru samples showed a continuous degradation during the CV test, indicating poor durability of Ru that cannot be employed as practical OER catalysts. After doping with Co, Cr, Zn, and Mn, CV curves of Ru-based catalysts were still suffering obvious degradation except RuMn, which showed robust stability after 10, 1000, 5000, 10 000, and even 20 000 CV cycles with almost coincident curves.

As mentioned above, RuMn exhibited distinguishable performance in consecutive CV scans. To confirm the durability of RuMn, electrochemical tests and inductivity-coupled plasma mass spectrometry (ICP-MS) were conducted on catalysts and electrolytes, respectively. As an accelerated degradation test, thousands of CV cycles test well mimic the start-up and shutdown cycles of electrolyzer operation. And the CP test is recommended as a straightforward way to demonstrate long-term stability.

LSV curves were derived by taking an average of the positive and negative-going scans of measured CV curves with Ir-correction. Over-potentials were recorded at $10 \text{ mA cm}_{\text{geo}}^{-2}$, which showed a highly steady activity with $\approx 10 \text{ mV}$ rise after 20 000 CV cycles. Considering that the leaching process on materials could lead to a changing surface area, which may conceal the real degradation process, the surface area variation should be detected. Electrochemical double-layer capacities (EDLC; Figure S4, Supporting Information) evolution during CV cycles was analyzed in Figure 3b, which shows a huge increase after the first 1000 cycles, followed by relatively steady EDLCs in subsequent CV tests. The sharp increase in EDLC could be attributed to the oxidation of RuMn alloy on the CFPs, since metal oxides own larger EDLC than metal alloys. What's more, along with continuous leaching of catalysts, inner layers could be exposed to participate in the reaction, thus providing a constant potential over extended times even though the material degrades. Testing the mass loss is a possible solution to rule out this possibility.^[12] In order to quantify the dissolution of RuMn, ICP-MS was used to test the concentration of Ru and Mn in the electrolyte. With accelerated aging tests, concentrations of Ru and Mn in the electrolyte (Figure 3c)

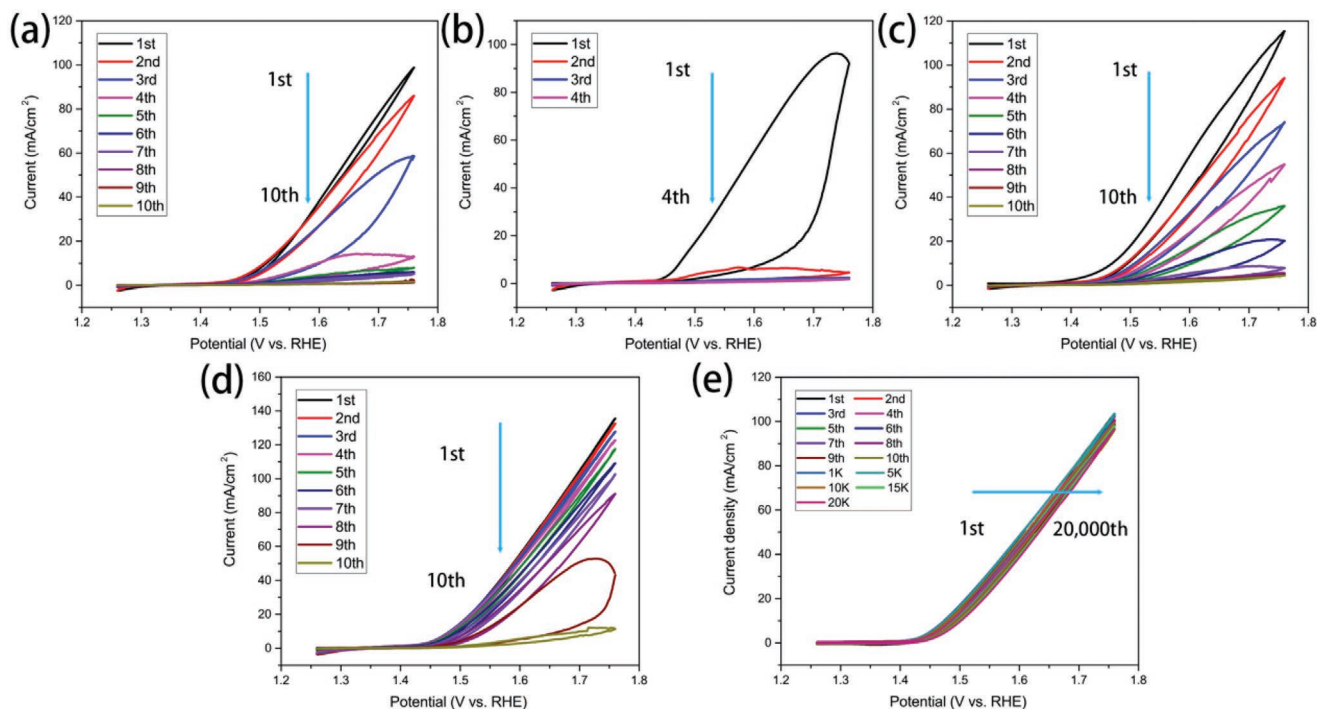


Figure 2. CV cycles of pristine a) Ru, b) RuCo, c) RuCr, d) RuZn, and e) RuMn.

showed an obvious growth after ten CV cycles followed by a small increase after 1000 CV cycles and a relatively stable value from 1000 to 20000 CV cycles. The concentration evolution indicated

that the rapid dissolution in the first ten cycles corresponding to the transient dissolution, and the steady-state dissolution has been suppressed from 1000 to 20000 cycles.

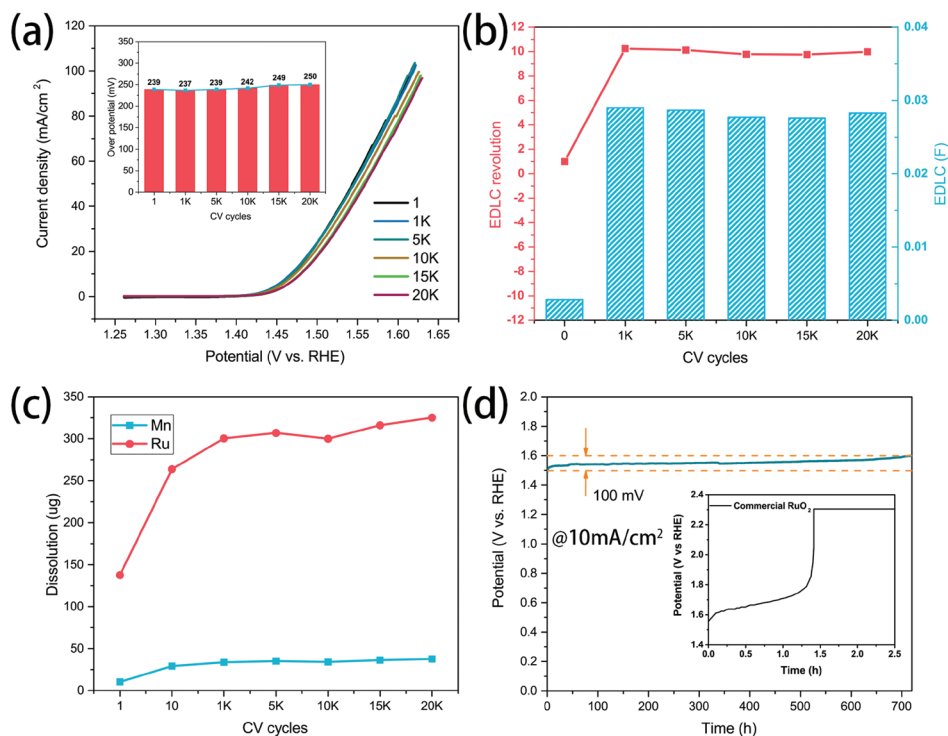


Figure 3. Electrochemical OER performance of the RuMn in 0.5 M H₂SO₄. a) Polarization curves after 85% iR-correction, b) EDLC revolution of pristine RuMn and after 1000, 5000, 10000, and 20000 cycles and c) Ru and Mn dissolution condition. d) The CP curve of RuMn (this work) and commercial RuO₂ at 10 mA cm⁻².

Table 1. Comparison of OER stable performance with some representative electrocatalysts in acidic media.^[8a,10c,14]

Catalysts	Electrolyte	Durability test time	Durability test standard	Voltage increase fraction	Voltage increase fraction per hour
RuMn (this work)	0.5 M H ₂ SO ₄	720 h	10 mA cm ⁻²	6.70%	0.093%
IrO _x /SrIrO ₃	0.5 M H ₂ SO ₄	30 h	Chronoamperometric*		
Y ₂ Ru ₂ O _{7-δ}	0.1 M HClO ₄	8 h	1 mA cm ⁻²		
Y _{1.8} Zn _{0.15} Ru ₂ O _{7-δ}	0.5 M H ₂ SO ₄	8 h	1 mA cm ⁻²		
RuTe ₂	0.5 M H ₂ SO ₄	24 h	Chronoamperometric*		
RuO ₂ nanosheets	0.1 M HClO ₄	6 h	1 mA cm ⁻²		
ultrafine defective RuO ₂	0.5 M H ₂ SO ₄	20 h	10 mA cm ⁻²	1.31%	0.66%
Ru-exchanged Cu-BTC	0.5 M H ₂ SO ₄	8 h	10 mA cm ⁻²	6.23%	7.79%
Cr _{0.6} Ru _{0.4} O ₂	0.5 M H ₂ SO ₄	10 h	10 mA cm ⁻²	4.22%	4.22%
Mn-doped RuO ₂	0.5 M H ₂ SO ₄	10 h	10 mA cm ⁻²	1.88%	1.88%
Co-doped RuO ₂	0.5 M H ₂ SO ₄	50 h	10 mA cm ⁻²	7.19%	1.44%
Mg-doped RuO ₂	0.5 M H ₂ SO ₄	30 h	10 mA cm ⁻²	6.94%	2.31%
RuO ₂ /(Co,Mn) ₃ O ₄	0.5 M H ₂ SO ₄	24 h	10 mA cm ⁻²	8.45%	3.52%
Amorphous/Crystalline RuO ₂	0.1 M HClO ₄	60 h	10 mA cm ⁻²	8.59%	1.43%
Donutlike RuCu	0.5 M H ₂ SO ₄	20 h	Chronoamperometric*		
Na-doped SrRuO ₃ perovskite	0.1 M HClO ₄	20 cycles	CV cycles		
Ru ₁ -Pt ₃ Cu	0.1 M HClO ₄	28 h	10 mA cm ⁻²	2.83%	1.01%

*Initial voltage was set at the potential under current density of 10 mA cm⁻².

Hence, the outstanding durability of RuMn is believed to be attributed to prohibit steady-state dissolution, which is also supported by the continuous dissolution of unstable Ru-M. Specifically, the ruthenium dissolution degree of unstable RuZn samples with CV scanning (Figure S5, Supporting Information) shows a constant increase verifying a continuous dissolution with obvious electrochemical performance degradation. SEM patterns of alloy samples before and after CV test comparison (Figure S2, Supporting Information) also illustrated that Ru and Ru-M (M = Co, Cr, Zn) catalysts suffering degradation in CV scanning were vanished on CFPs due to the severe dissolution. By contrast, RuMn is still on the CFPs, and the morphology remains unchanged before and after 1000 CV cycles (Figure S2e2,e3, Supporting Information). Research has revealed that Ru-based catalysts undergo a more violent steady-state dissolution than transient dissolution. Doping with Mn had significantly helped RuMn alloy to be stable on the substrate, preventing the steady-state dissolution during the CV cycle tests.

CP measurement performed at 10 mA cm⁻² has been suggested as a benchmark OER stability testing condition. For acidic media, most literature research reported the durability test within 50 h. While Chen et al. had recommended that the long-term stability, OER catalysts should operate by CA or CP tests for at least hundreds of hours combined with dissolution species measurement.^[13] By comparison, in this research, RuMn has achieved 720 h of stable performance in CP test (Figure 3d) that is the best activity among the reported OER catalysts in acidic media (Table 1).

To better explore the mechanism of RuMn alloy with robust stability, TEM images (Figure 4) of samples before and after the CV test were obtained. Compared with pristine particles (Figure 4a), RuMn alloy after 1000 CV cycle-test in Figure 4c

shows an obvious loose shell of the particles. EDS analysis of the tested particle was carried on the line across particles. Along the yellow line, Ru and Mn intensities showed a similar intensity trend in the pristine particle while Mn intensity signal was not detected until 45–70 nm deep in the tested particle (Figure 4d). Figure 4d suggests that the Ru intensity can be detected in the particle shell, indicating the shell formed after the CV cycles only contain Ru elements while Mn elements have been leached. XPS spectra of RuMn in Figure S7 (Supporting Information) reveal that Mn 2p peaks disappear after 1000 CV cycles, also prove the formation of a shell only composed of ruthenium metal.

Due to the high anodic current for OER, studies have shown that surface of bulk Ru metal would be oxidized into RuO₂ during the catalytic process. XPS spectra of RuMn samples before and after CV cycles have been analyzed to probe the electronic interaction of Ru (Figure S8, Supporting Information). Considering the overlap of C 1s and Ru 3d_{3/2} peaks, Ru 3p peaks were used to determine the Ru electronic structure. Ru 3p peaks were deconvoluted into two sets of doublet peaks of Ru 3p_{3/2} and Ru 2p_{1/2} with a spin-orbit splitting of 22.4 eV. For pristine RuMn alloy, the main peaks at 462.01 and 484.41 eV are associated with Ru 3p_{1/2} and Ru 3p_{3/2}, respectively. After electrochemical accelerated degradation tests, these peaks shift to higher binding energies, which show 1.2 and 0.12 eV upshift of RuMn after 1000 and 10000 CV cycles test, respectively. The positive shift of Ru 3p binding energy (B.E.) indicates Ru has been oxidized to a higher valence state during the CV cycles. The peaks at 465.346 and 487.746 eV are assigned to Ru⁴⁺ species. A higher Ru⁴⁺ species content can be observed during the ADTs that also reveals the oxidation of surface Ru, and a RuO_x surface have been formed.

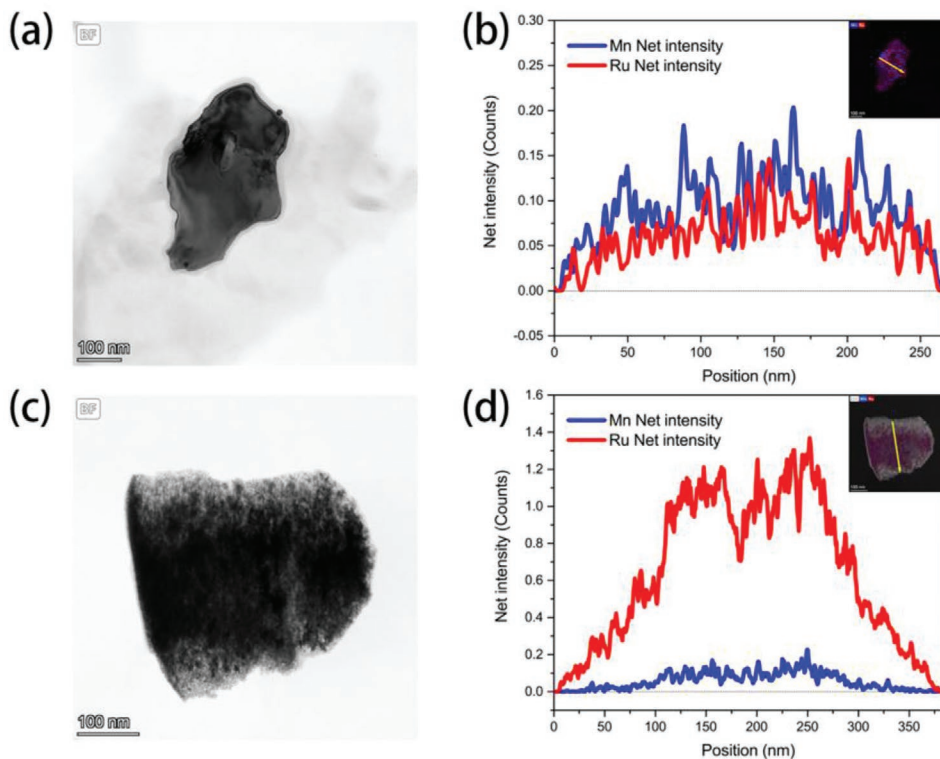


Figure 4. TEM images and elements distribution along the line of RuMn@CFPs a,b) before and c,d) after CV scanning.

Furthermore, the crystallization of RuO_x shell was deeply investigated. XRD pattern of RuMn after 10000 CV cycles (Figure 5a) shows a weak peak without any characteristic peak. Raman spectra (Figure S9, Supporting Information) also have no visible intensity in 0–1000 Raman shift where generally crystalline oxides show peaks in this area. Evidence from XRD and Raman document that the RuO_x shell did not have a crystalline structure but was composed of amorphous RuO_x. The HRTEM pattern (Figure S10, Supporting Information) also confirms the amorphous-shell and crystalline-core structure. The amorphization could be initiated by the lattice oxygen redox with electrochemical measurement.^[15] Hence, the amorphous RuO_x was supposed to be constructed during the surface reconstruction by the dealloying treatment. Interestingly, amorphous catalysts

are flexible with respect to structural distortions that have shown a remarkable electrochemical catalytic performance with an improved durability in OER. However, few explorations have been focused on the amorphous form of RuO_x. The initial work available on amorphous RuO₂ applied to OER electrolysis had emphasized that the promotion of activity is probably attributed to the structural flexibility that is characteristic of the amorphous surface.^[16] An amorphous/crystalline RuO₂ has been reported as a robust pH-Universal oxygen evolution electrocatalyst benefiting from the amorphous.^[14k] The field of acidic water oxidation electrocatalysis is relatively underdeveloped, and RuO₂ is not explored much in its amorphous form. Researchers have investigated that the flexible structure of the amorphous surface can inhibit the steady-state dissolution

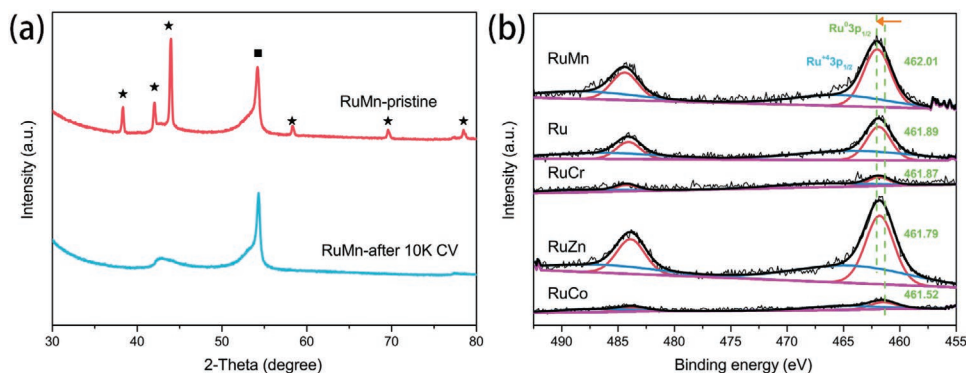


Figure 5. a) XRD patterns of RuMn before and after 10000 CV cycles; b) XPS spectra of pristine Ru, RuCr, RuCo, RuZn, and RuMn.

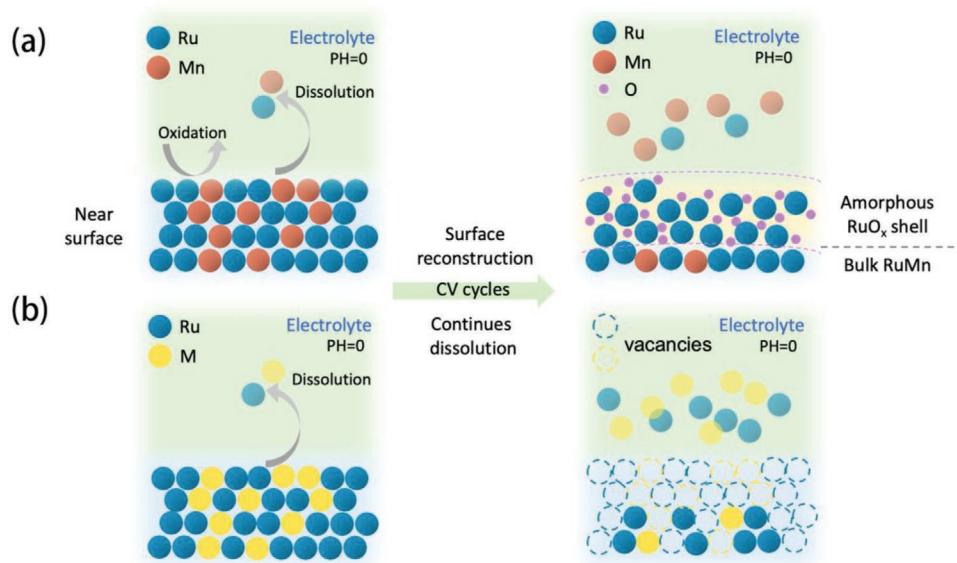


Figure 6. Schematic of surface reconstruction for a) RuMn and dissolution for b) unstable Ru-based alloys in acidic media during CV cycles.

of Ru by preventing the over-oxidation of Ru. Wang et.al have pointed out that the structural flexibility allows materials to self-regulate themselves withstand structural according to the electrocatalytic conditions.^[14c] The control of the redox reaction of Ru and surface structure has dramatically enhanced the stability of RuMn catalyst in OER.

Considering the different mechanism schematic of RuMn and other unstable Ru-based samples, XPS was performed to further investigate the electronic interaction. In the Ru 3p spectra (Figure 5b), Ru 3p peaks were deconvoluted into two sets of doublet peaks for Ru 3p_{1/2} and Ru 3p_{3/2} and their satellite peaks.^[10c,17] Compared with Ru, Ru 3p peak of RuMn shifts to higher BE at 462.01 eV, indicating that Mn has a stronger effect on the electron structure of Ru. By contrast, RuZn and RuCr samples showed slight shifts compared with Ru. Moreover, RuCo presented the lowest BE.

As shown in the schematic (Figure 6), during the electrooxidation of RuMn under anodic CV scan, except the OER process, the Ru and Mn elements would preliminary be oxidized and dissolved. The surface transformation is triggered by partial cation leaching, which is driven by the corrosive chemical environment and the high anodic potential. Studies have shown that the surface transformation level of catalyst is influenced by the lattice instability, proposing that materials with a lower coordination number or lower bond strength can reconstruct more readily.^[18] While the transformation level should be controllable to be terminated at a stable oxide layer instead of endless leaching.^[19] Here, the stronger bond energy of RuMn benefits RuMn to go through a moderate dissolution, which facilitates further oxidation and the insertion of oxygen atoms and transforms surface RuO_x into a highly disordered network. Consequently, a stable amorphous surface is formed to protect the inner alloy.^[15] And for other Ru-based samples, lower bond strength makes them suffer a severe dissolution without a termination. A previous study had summarized the Ru be oxidized could be more stable to be left in the final product.^[6]

What's more, the XPS analysis of RuMn during the CV cycles (Figure S7, Supporting Information) also reveals obvious upshift of Ru 3p with the RuMn transferred into core-shell structure under the first 10000 CV cycles. And, there is a small upshift of Ru 3p BE from 10000 to 100000 cycles, indicating that the RuMn is transferred to a stable state during the electrochemical test and the stronger M–M bond strength would be more facile for the structure stability.

For the support of density functional theory (DFT), additional evidence of the degeneration process proves the high stability of RuMn in this simplified model. Figure S12 (Supporting Information) shows the energy change when the Ru surface is dissolved at a different potential. The U_{diss} of Ru, Ru₃Cr, Ru₇Mn, and RuCo are 0.45, 0.45, 0.51, and 0.35 V. It is suggested that the Ru₇Mn performs the best stability, and the stabilities of Ru₃Cr and RuCo are lower than that of Ru slab. In other words, the Mn element is helpful to stabilize the Ru surface. Considering the differences between the real electrochemical environment and the calculate model, the U_{diss} could be used to measure the relative durability difference. Figure 7 concludes that there could be a positive correlation between durability and BE of Ru, indicating a higher BE could lead to a more stable Ru-based electrocatalyst under the acidic OER.

In summary, surface engineering with dealloying has been applied to Ru-based alloys to boost higher durability. Among them, RuMn exhibits excellent resistance to acid corrosion and oxidation in OER while other Ru-based samples suffered from severe dissolution. The RuMn alloy displays very competitive OER durability detected by the CP test of 720 h, which significantly improves the durability from 10 h of most available OER electrocatalysts in acidic condition. An amorphous RuO_x shell was formed on the surface when RuMn underwent OER electrochemical test. The electronic interaction investigation has been proposed that the successful reconstruction of RuMn could be attributed to the higher bond strength of Ru tuned by

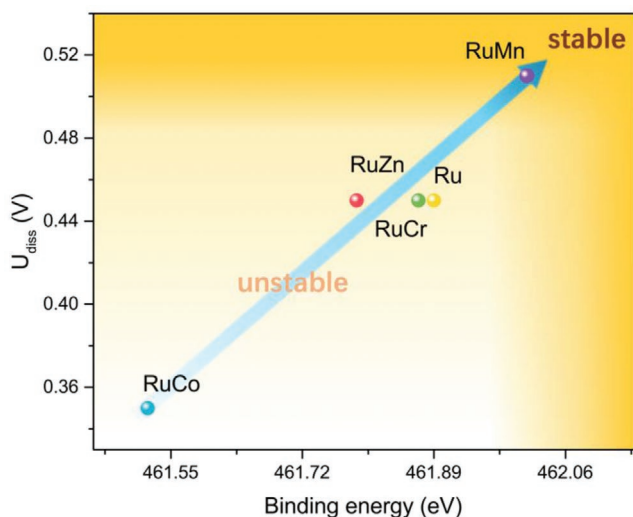


Figure 7. Durability-B.E. (Ru) relationships found in this study.

doping with Mn. This work suggests the surface reconstruction can provide hints for the design strategies for stable OER catalysts, and stronger bond strength of Ru regulated by doping is beneficial to self-terminating reconstruction.

3. Experimental Section

Preparation of Electrocatalysts: Commercial carbon fiber paper (CFP) was used as a substrate. Before deposition, CFP was cut into pieces of 1×2 cm and washed in ethanol. Ruthenium (III) chloride hydrate ($\text{RuCl}_3 \cdot x\text{H}_2\text{O}$; 145.2 mg) and 0.16 g PVP (MW = 360000) (Aladdin Industrial Corp) were dissolved into 3 mL deionized water (18.2 M Ω). The alien atom to Ru atomic ratio was kept at 1:1. 0.7 mmol Cobalt(II) nitrate hexahydrate ($\text{Co}(\text{NO}_3)_2 \cdot 6\text{H}_2\text{O}$), manganese (II) chloride tetrahydrate ($\text{MnCl}_2 \cdot 4\text{H}_2\text{O}$), chromium (III) chloride hexahydrate ($\text{CrCl}_3 \cdot 6\text{H}_2\text{O}$), and zinc (II) nitrate hexahydrate ($\text{Zn}(\text{NO}_3)_2 \cdot 6\text{H}_2\text{O}$) were added into above-mixed solvent separately and then stirred overnight before loading. All the reagents for synthesis were commercially available. The dip-coating method was applied to direct synthesis electrode with catalysts in situ grown on the substrate.^[8e,11] CFPs were dipped into the precursor solution for 10 s and then dried in a vacuum oven at 50 °C. After drying for 20 min, CFPs were transferred into a tube furnace and heated in a hydrogen atmosphere room temperature to 800 °C for 7 h (ramping rate: 5 °C min⁻¹).

Characterizations: X-ray diffraction (XRD) patterns were collected on a mini Flex Guidance with Cu K α radiation ($\lambda = 1.5406$ nm \AA). Scanning electron microscopic (SEM) images were obtained on Mira3 LHM at 5 kV. Transmission electron microscopic (TEM) and HADDF-STEM&EDS images were acquired on Talos F200X G2. X-ray photoelectron spectroscopy (XPS) measurements were carried out on AXIS Ultra DLD spectrometer, using a monochromatic Al K α radiation with a low-energy flood gun as a neutralizer. The BEs of samples were calibrated by referencing the C 1s peak at 284.8 eV. Raman spectra were conducted on RISE-MAGNA. The dissolution of Ru in the electrolyte was determined by ICP analysis. Inductivity coupled plasma mass spectrometry (ICP-MS) was performed on NexION2000 (Flexar20 HPLC).

Electrochemical Characterization: Electrochemical measurements were carried out in a three-electrode cell at room temperature with CHI 660E electrochemical analyzer (CH instrument, Inc., Shanghai). For the working electrode, RuM@CFP was fixed by a titanium electrode clamp. Carbon rod and a saturated calomel electrode (SCE) were used as counter and reference electrodes, respectively.

The linear sweep voltammograms (LSV) for OER were recorded by CV at the potential range of 1.25–1.75 V (vs reversible hydrogen electrode, RHE) in 0.5 M H_2SO_4 . ADTs were carried out between 1.0 and 1.4 V versus SCE under a scan rate of 0.5 V s⁻¹. Chronopotentiometry measurement was performed at a constant current density of 10 mA cm⁻².

Supporting Information

Supporting Information is available from the Wiley Online Library or from the author.

Acknowledgements

This work was supported by the National Natural Science Foundation of China (No. 21975157 and 22002089) and the Oceanic Interdisciplinary Program of Shanghai Jiao Tong University (No. SL2021ZD105).

Conflict of Interest

The authors declare no conflict of interest.

Data Availability Statement

The data that support the findings of this study are available from the corresponding author upon reasonable request.

Keywords

acidic environment, durability, oxygen evolution reaction, ruthenium-based

Received: January 5, 2022

Revised: March 20, 2022

Published online:

- [1] a) M. Carmo, D. L. Fritz, J. Mergel, D. Stolten, *Int. J. Hydrogen Energy* **2013**, *38*, 4901; b) S. Cherevko, A. R. Zeradjanin, A. A. Topalov, N. Kulyk, I. Katsounaros, K. J. Mayrhofer, *ChemCatChem* **2014**, *6*, 2219; c) N. Armaroli, V. Balzani, *Angew. Chem., Int. Ed.* **2007**, *46*, 52.
- [2] N.-T. Suen, S.-F. Hung, Q. Quan, N. Zhang, Y.-J. Xu, H. M. Chen, *Chem. Soc. Rev.* **2017**, *46*, 337.
- [3] a) J. Shan, Y. Zheng, B. Shi, K. Davey, S.-Z. Qiao, *ACS Energy Lett.* **2019**, *4*, 2719; b) Z. Chen, X. Duan, W. Wei, S. Wang, B.-J. Ni, *Nano Energy* **2020**, *78*, 105392; c) Z. Lei, T. Wang, B. Zhao, W. Cai, Y. Liu, S. Jiao, Q. Li, R. Cao, M. Liu, *Adv. Energy Mater.* **2020**, *10*, 2000478.
- [4] K. Macounova, M. Makarova, P. Krtil, *Electrochem. Commun.* **2009**, *11*, 1865.
- [5] T. Binninger, R. Mohamed, K. Waltar, E. Fabbri, P. Levecque, R. Kötzt, T. J. Schmidt, *Sci. Rep.* **2015**, *5*, 12167.
- [6] N. Hodnik, P. Jovanovič, A. Pavlišič, B. Jozinovič, M. Zorko, M. Bele, V. S. Šelih, M. Šala, S. Hočvar, M. Gaberšček, *J. Phys. Chem. C* **2015**, *119*, 10140.
- [7] H. Ding, H. Liu, W. Chu, C. Wu, Y. Xie, *Chem. Rev.* **2021**.
- [8] a) L. C. Seitz, C. F. Dickens, K. Nishio, Y. Hikita, J. Montoya, A. Doyle, C. Kirk, A. Vojvodic, H. Y. Hwang, J. K. Nørskov, *Science* **2016**, *353*, 1011; b) A. Grimaud, A. Demortière, M. Saubanière, W. Dachraoui, M. Duchamp, M.-L. Doublet, J.-M. Tarascon, *Nat.*

- Energy* **2016**, *2*, 1; c) H. N. Nong, T. Reier, H.-S. Oh, M. Gliech, P. Paciok, T. H. T. Vu, D. Teschner, M. Heggen, V. Petkov, R. Schlögl, *Nat. Catal.* **2018**, *1*, 841; d) H. Guo, Z. Fang, H. Li, D. Fernandez, G. Henkelman, S. M. Humphrey, G. Yu, *ACS Nano* **2019**, *13*, 13225; e) L. An, X. Cai, S. Shen, J. Yin, K. Jiang, J. Zhang, *Dalton Trans.* **2021**, *50*, 5124; f) R. Zhang, N. Dubouis, M. Ben Osman, W. Yin, M. T. Sougrati, D. A. Corte, D. Giaume, A. Grimaud, *Angew. Chem.* **2019**, *131*, 4619.
- [9] K. Jiang, M. Luo, M. Peng, Y. Yu, Y.-R. Lu, T.-S. Chan, P. Liu, F. M. de Groot, Y. Tan, *Nat. Commun.* **2020**, *11*, 1.
- [10] a) M. Aizaz Ud Din, S. Irfan, S. U. Dar, S. Rizwan, *Chemistry – A European Journal* **2020**, *26*, 5662; b) M. Huynh, D. K. Bediako, D. G. Nocera, *J. Am. Chem. Soc.* **2014**, *136*, 6002; c) S. Chen, H. Huang, P. Jiang, K. Yang, J. Diao, S. Gong, S. Liu, M. Huang, H. Wang, Q. Chen, *ACS Catal.* **2019**, *10*, 1152.
- [11] K. Jiang, H. Wang, W.-B. Cai, H. Wang, *ACS Nano* **2017**, *11*, 6451.
- [12] a) R. Frydendal, E. A. Paoli, B. P. Knudsen, B. Wickman, P. Malacrida, I. E. Stephens, I. Chorkendorff, *ChemElectroChem* **2014**, *1*, 2075; b) S. Geiger, O. Kasian, A. M. Mingers, S. S. Nicley, K. Haenen, K. J. Mayrhofer, S. Cherevko, *ChemSusChem* **2017**, *10*, 4140.
- [13] F.-Y. Chen, Z.-Y. Wu, Z. Adler, H. Wang, *Joule* **2021**.
- [14] a) J. Kim, P.-C. Shih, K.-C. Tsao, Y.-T. Pan, X. Yin, C.-J. Sun, H. Yang, *J. Am. Chem. Soc.* **2017**, *139*, 12076; b) Q. Feng, Q. Wang, Z. Zhang, Y. Xiong, H. Li, Y. Yao, X.-Z. Yuan, M. C. Williams, M. Gu, H. Chen, *Appl. Catal., B* **2019**, *244*, 494; c) J. Wang, L. Han, B. Huang, Q. Shao, H. L. Xin, X. Huang, *Nat. Commun.* **2019**, *10*, 1; d) S. Laha, Y. Lee, F. Podjaski, D. Weber, V. Duppel, L. M. Schoop, F. Pielhofer, C. Scheurer, K. Müller, U. Starke, *Adv. Energy Mater.* **2019**, *9*, 1803795; e) R. Ge, L. Li, J. Su, Y. Lin, Z. Tian, L. Chen, *Adv. Energy Mater.* **2019**, *9*, 1901313; f) J. Su, R. Ge, K. Jiang, Y. Dong, F. Hao, Z. Tian, G. Chen, L. Chen, *Adv. Mater.* **2018**, *30*, 1801351; g) Y. Lin, Z. Tian, L. Zhang, J. Ma, Z. Jiang, B. J. Deibert, R. Ge, L. Chen, *Nat. Commun.* **2019**, *10*, 1; h) Y. Tian, S. Wang, E. Velasco, Y. Yang, L. Cao, L. Zhang, X. Li, Y. Lin, Q. Zhang, L. Chen, *Science* **2020**, *23*, 100756; i) Z. Li, S. Wang, Y. Tian, B. Li, H. Jun Yan, S. Zhang, Z. Liu, Q. Zhang, Y. Lin, L. Chen, *Chem. Commun.* **2020**, *56*, 1749; j) S. Niu, X.-P. Kong, S. Li, Y. Zhang, J. Wu, W. Zhao, P. Xu, *Appl. Catal., B* **2021**, *297*, 120442; k) L. Zhang, H. Zhang, H. Liu, M. G. Kim, D. Yang, S. Liu, X. Liu, J. Cho, *Angew. Chem., Int. Ed.* **2021**; l) Y. Li, W. Zhou, X. Zhao, W. Cheng, H. Su, H. Zhang, M. Liu, Q. Liu, *ACS Appl. Energy Mater.* **2019**, *2*, 7483; m) M. Retuerto, L. Pascual, F. Calle-Vallejo, P. Ferrer, D. Gianolio, A. G. Pereira, Á. García, J. Torrero, M. T. Fernández-Díaz, P. Bencok, *Nat. Commun.* **2019**, *10*, 2041; n) Y. Yao, S. Hu, W. Chen, Z.-Q. Huang, W. Wei, T. Yao, R. Liu, K. Zang, X. Wang, G. Wu, *Nat. Catal.* **2019**, *2*, 304.
- [15] G. Wan, J. W. Freeland, J. Kloppenburg, G. Petretto, J. N. Nelson, D.-Y. Kuo, C.-J. Sun, J. Wen, J. T. Diulus, G. S. Herman, *Sci. Adv.* **2021**, *7*, eabc7323.
- [16] E. Tsuji, A. Imanishi, K.-i. Fukui, Y. Nakato, *Electrochim. Acta* **2011**, *56*, 2009.
- [17] Y. Wen, T. Yang, C. Cheng, X. Zhao, E. Liu, J. Yang, *Chin. J. Catal.* **2020**, *41*, 1161.
- [18] G. Somorjai, M. Van Hove, *Catal. Lett.* **1988**, *1*, 433.
- [19] T. Wu, S. Sun, J. Song, S. Xi, Y. Du, B. Chen, W. A. Sasangka, H. Liao, C. L. Gan, G. G. Scherer, *Nat. Catal.* **2019**, *2*, 763.
- [20] a) G. Kresse, J. Hafner, *Phys. Rev. B* **1993**, *47*, 558; b) G. Kresse, J. Hafner, *Phys. Rev. B* **1994**, *49*, 14251; c) G. Kresse, J. Furthmüller, *Comput. Mater. Sci.* **1996**, *6*, 15; d) G. Kresse, J. Furthmüller, *Phys. Rev. B* **1996**, *54*, 11169.
- [21] a) G. Kresse, D. Joubert, *Phys. Rev. B* **1999**, *59*, 1758; b) P. E. Blöchl, *Phys. Rev. B* **1994**, *50*, 17953.
- [22] a) B. Hammer, J. K. Nørskov, *Nature* **1995**, *376*, 238; b) J. K. Nørskov, T. Bligaard, A. Logadottir, J. Kitchin, J. G. Chen, S. Pandelov, U. Stimming, *J. Electrochem. Soc.* **2005**, *152*, J23.